Slow Dielectric Relaxation of Entangled Linear *cis*-Polyisoprenes with Asymmetrically Inverted Dipoles. 2. Behavior in a Short Matrix†

Hiroshi Watanabe,* Osamu Urakawa, and Tadao Kotaka

Department of Macromolecular Science, Faculty of Science, Osaka University, Toyonaka, Osaka 560, Japan

Received January 13, 1994; Revised Manuscript Received April 2, 1994•

ABSTRACT: For a series of *cis*-polyisoprene (PI) chains having almost identical molecular weights ($M \simeq$ 48K) but differently inverted type-A dipoles parallel along the chain contour, dielectric relaxation behavior was examined in *homogeneous* blends with a polybutadiene matrix (B-9; M = 9K). In the blends, the PI chains were dilute and entangled only with the shorter B-9 matrix. This matrix was dielectrically inert, and the dielectric loss (ϵ'') of the blends was attributed to global motion of the PI chains having type-A dipoles. Because of the differences of the location of the dipole inversion points, the PI chains of almost identical M exhibited remarkably different ϵ'' curves. As the inversion point shifted from the chain end to the center, the curve shifted to the higher frequency (ω) side and the relaxation mode distribution became first broader and then narrow again. Those PI chains relaxed locally as the shorter matrix B-9 chains rapidly diffused away and globally by accumulating such local processes. For this type of relaxation generally referred to as *constraint release* (CR) relaxation, the ϵ'' data enabled us to evaluate low-order eigenfunctions $f_p(n)$ (with the mode number p = 1–3) for a local correlation function, $C(n,t;m) = (1/a^2)\langle \mathbf{u}(n,t)\cdot\mathbf{u}(m,0)\rangle$ ($\mathbf{u}(n,t)$ = nth bond vector at time t and $a^2 = \langle \mathbf{u}^2\rangle$). Those $f_p(n)$ were not largely but certainly different from sinusoidal eigenfunctions $f_p^\circ(n)$ deduced from a conventional CR model *assuming Rouse nature of CR processes*. This Rouse CR model was further examined for an orientation function $S(n,t) = (1/a^2)\langle u_x(n,t)u_y(n,t)\rangle$ that describes fundamental features of viscoelastic relaxation. For CR relaxation, $S(n,t)$ can be generally expanded with respect to the *dielectrically determined* functions, $[f_p(n)]^2$. Storage moduli, G' and $G^{\circ\prime}$, were thus calculated at low ω from the experimental f_p and model f_p°, respectively. Corresponding to the difference between f_p and f_p°, G' was not extremely but certainly larger than $G^{\circ\prime}$ at intermediate to high ω. This result was in harmony with viscoelastic data for long and dilute probe chains entangled with much shorter matrices, meaning that the dielectric and viscoelastic relaxation processes of such probe chains are consistently described by a non-Rouse type CR mechanism. Differences between the actual CR behavior and the prediction of the Rouse CR model were discussed in relation to extra relaxation at the chain ends that was not considered in the model.

I. Introduction

For investigation of the entanglement dynamics[1,2] of flexible chains, blends of *dilute* probe chains in matrices of various length are important model systems. In such blends, a lifetime of entanglement for the probe is determined by global motion (diffusion) of the matrix chains. Extensive experiments[3–12] have indicated that the probe behavior changes with this lifetime and thus with the matrix molecular weight M_{mat} in the following way. When the lifetime is sufficiently long (for large M_{mat}), the probe relaxation is completed before it is affected by the matrix motion. In this extreme case, the probe relaxation is independent of M_{mat} and determined only by its own molecular weight M_{probe}. On the other hand, in the other extreme of short matrices (that are still long enough to be entangled with the probe), rapid matrix motion induces local relaxation of the probe, and accumulation of such local processes leads to global (terminal) relaxation of the probe that is dependent on both M_{mat} and M_{probe}. Thus, the relaxation mechanisms are quite different for these two cases, and competition of these mechanisms determines the probe relaxation in matrices of intermediate M_{mat}.

In modified tube models[13–17] frequently used for describing relaxation in entangled blends, the above two extreme mechanisms are involved as the reptation and constraint-release mechanisms, respectively, and the latter has been further assumed to have Rouse nature.[15–17] Those models reasonably well describe general features of the probe relaxation behavior, but nonnegligible disagreements still exist, for example, for mode distribution of relaxation functions[5,6,12] that reflects details of the probe motion. It is of particular interest to study those details *in a purely experimental way*. For this purpose, it is essential to use some labeling techniques, like isotope labeling successfully used in diffusion[8] and orientation relaxation[18,19] experiments, and examine various dynamic quantities for a particular segment and/or chain in the system. Recently, we have demonstrated that *dipole inversion* is a powerful and important dielectric labeling technique.[12,20,21]

As pioneered by Stockmayer and co-workers[22,23] and later examined extensively by several groups,[11,12,20,21,24–29] global motion of *type-A* chains having dipoles parallel along the contour induces M-dependent, slow dielectric relaxation. For a special sort of type-A chains having once-inverted dipoles, the dielectric relaxation is related to fluctuation of a vector $\Delta\mathbf{R} = \mathbf{R}_1 - \mathbf{R}_2$, with $\mathbf{R}_1$ and $\mathbf{R}_2$ being the vectors that connect the inversion point and the chain ends (cf. Figure 1).[6,12,20,21] Thus, the chains having differently inverted dipoles exhibit different dielectric responses even if their motion is the same. Such responses provide detailed information on the correlation of chain orientation at two separate times.[21] In this sense, the dipole inversion works as the dielectric labeling. Another sort of dielectric labeling, linkage of chemically different type-A and non-type-A blocks, unavoidably introduces a stepwise distribution of segmental friction and entangle-

† Dedicated to Professor Walter H. Stockmayer on the occasion of his 80th birthday. A part of this work was presented at the Stockmayer Symposium in ACS San Diego Meeting, March 1994.

• Abstract published in *Advance ACS Abstracts*, May 15, 1994.

0024-9297/94/2227-3525$04.50/0

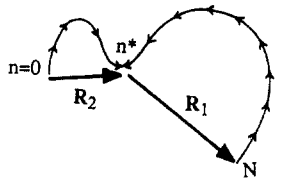

Figure 1. Schematic representation of a PI chain having asymmetrically inverted dipoles.

ment spacing along the contour of the resulting block copolymers, unless one of the two blocks is extremely shorter than the other. This distribution affects the chain motion, and the dielectric data of such copolymers[27] do not provide clear and quantitative information for homopolymer dynamics. The use of dipole-inverted homopolymers is essential for obtaining this information.

On the basis of the above idea, our previous work was devoted for a study of dielectric relaxation of monodisperse bulk systems of entangled *cis*-polyisoprene (PI) chains having almost identical molecular weights (≅48K) but differently inverted parallel dipoles.[21] Analyzing their dielectric data, we evaluated eigenfunctions for a local correlation function $C(n,t;m)$ that describes orientation correlation of n and mth segments at two separate times t and 0. The experimental eigenfunctions were not largely but certainly different from sinusoidal eigenfunctions deduced from conventional modified tube models. This difference was related to some relaxation mechanism enhanced at chain ends.

Monodisperse systems are classified as special cases of blends composed of the probe and matrix chains having the same molecular weight. In the above PI systems with $M \cong 48$K, the entanglement lifetime was relatively long and the probe relaxation was not significantly affected by the matrix motion. In relation to the extensive data we have accumulated for blends,[3-6,12] it is of our particular interest to study the behavior of the dilute probes in a matrix of much shorter lifetime, too.

From this point of view, we have studied dielectric relaxation behavior for *homogeneous* blends of the dipole-inverted PI probes entangled with a short polybutadiene (PB) matrix. This paper presents the results. First, section II explains the theoretical background for (1) the determination of eigenfunctions for $C(n,t;m)$ and (2) the relationship between dielectric and viscoelastic quantities of type-A chains. Then, section III describes experimental methods, and section IV, dielectric data and resulting eigenfunctions. Finally, section V discusses (1) differences of relaxation processes in monodisperse systems and blends, (2) detailed features of constraint-release (CR) processes and the relationship between dielectric and viscoelastic quantities, and (3) possible factors that determine the CR features. Readers who are interested in the comparison of dielectric and viscoelastic quantities may proceed directly from section II-2 to V-2.

II. Theoretical Section

II-1. Determination of Eigenfunctions. We consider dilute, linear, Gaussian chains, each having N *entanglement segments*, as the probe (PI) chains in a dielectrically inert matrix. For the probe chain having dipole inversion at the n^*th segment, slow dielectric relaxation is induced by fluctuation of the difference vector $\Delta\mathbf{R}(t) = \mathbf{R}_1(t) - \mathbf{R}_2(t)$ depicted in Figure 1. As a quantity that describes fundamental aspects of this relaxation, we introduce a local correlation function[12,13,21]

$$C(n,t;m) = (1/a^2)\langle \mathbf{u}(n,t)\cdot\mathbf{u}(m,0)\rangle \quad (1)$$

with $\mathbf{u}(n,t)$ being a bond vector for the nth segment at time t and $a^2 = \langle \mathbf{u}^2\rangle$. This function represents an orientation correlation of two bond vectors at separate times. The dielectric relaxation function $\Phi(t;n^*)$ (normalized to unity at $t = 0$) and dielectric loss factor $\epsilon''(\omega;n^*)$ of the probe are related to $C(n,t;m)$ as[12,21,30]

$$\Phi(t;n^*) = \frac{\langle \Delta\mathbf{R}(t)\cdot\Delta\mathbf{R}(0)\rangle}{\langle R_e^2\rangle} = \frac{1}{N}[\int_0^{n^*} dn - \int_{n^*}^{N} dn][\int_0^{n^*} dm - \int_{n^*}^{N} dm]\, C(n,t;m) \quad (2)$$

and

$$\epsilon''(\omega;n^*) = -\Delta\epsilon \int_0^\infty \frac{\partial\Phi(t;n^*)}{\partial t} \sin \omega t \, dt \quad (3)$$

Here, $\langle R_e^2\rangle$ is the mean-square end-to-end distance of the probe; ω, the angular frequency; and $\Delta\epsilon$, the dielectric relaxation intensity. Note that interchain correlation $\langle \Delta\mathbf{R}_j(t)\cdot\Delta\mathbf{R}_k(0)\rangle$ does not exist between *dilute* probes j and k, and eq 2 involves only the single-chain autocorrelation $\langle \Delta\mathbf{R}(t)\cdot\Delta\mathbf{R}(0)\rangle$ (for $j = k$).

Using eqs 2 and 3, we can analyze the n^*-dependent ϵ'' data of the dipole-inverted PI chains to find features of $C(n,t;m)$, i.e., how the bond orientation correlation changes with time. Details of analyses were explained previously,[21] and we here summarize the results. At long time scales, $C(n,t;m)$ is generally expanded with respect to its *eigenfunctions* $f_p(n)$ (with the mode number p) in a form[21]

$$C(n,t;m) = \frac{2}{N}\sum_{p=1}^{N} f_p(n)\, f_p(m) \exp(-t/\tau_p) \quad (4)$$

Here, τ_p is the pth relaxation time (=reciprocal of the pth eigenvalue; cf. eq 20). Equivalence of two chain ends allows us to classify f_p in two categories, odd $f_p(n)$ (with $p = 1, 3, \ldots$) satisfying a relation $f_p(n) = f_p(N - n)$ and even f_p (with $p = 2, 4, \ldots$) satisfying $f_p(n) = -f_p(N-n)$.[21] Random orientation at chain ends leads to a boundary condition for those f_p (and for C),

$$f_p(0) = f_p(N) = 0 \quad (5)$$

and the Gaussian chain conformation provides a normalization condition for f_p (=initial condition for C),

$$\frac{2}{N}\sum_{p=1}^{N} f_p(n)\, f_p(m) = \delta_{nm} = \frac{2}{N}\sum_{p=1}^{N} \sin\frac{p\pi n}{N} \sin\frac{p\pi m}{N} \quad (6)$$

As seen from eqs 2–4, ϵ'' is decomposed into modes,

$$\epsilon''(\omega;n^*) = \sum_{p=1}^{N} g_p(n^*) \frac{\omega\tau_p}{1 + \omega^2\tau_p^2} \quad (7)$$

where g_p represents the dielectric intensity of the pth mode. From g_p and the total relaxation intensity $\Delta\epsilon$, an integral of f_p defined by

$$F_p(n^*) = \frac{\sqrt{2}}{N}\int_0^{n^*} f_p(n)\, dn \quad (8)$$

is evaluated, *without assuming any molecular model*, as

$$F_p(N/2) - F_p(n^*) = \pm[g_p(n^*)/4\Delta\epsilon]^{1/2};\quad p = \text{odd} \quad (9a)$$

and

$$F_p(n^*) = \pm[g_p(n^*)/4\Delta\epsilon]^{1/2};\quad p = \text{even} \tag{9b}$$

As explained previously,[21] the sign in the right-hand sides of eq 9 is determined from a requirement of smooth and continuous n^* dependence of $F_p(n^*)$ for the series of dipole-inverted PI chains having narrowly spanned n^* values (cf. Table 1).

II-2. Relationship between Dielectric and Viscoelastic Quantities. Viscoelastic stress of a probe chain is related to the bond orientation anisotropy,[13-15] and we consider the anisotropy decay after imposition of a small step shear strain. The decay is described for an orientation function[6,13-15]

$$S(n,t) = (1/a^2)\langle u_x(n,t)u_y(n,t)\rangle \tag{10}$$

with $u_\alpha(n,t)$ being the α (=x,y) component of the bond vector for the nth entanglement segment of the probe chain. (The shear and shear-gradient directions are chosen as the x and y directions.) In general, $S(n,t)$ satisfies initial and boundary conditions representing uniform deformation at $t = 0$ and random orientation at chain ends,

$$S(n,0) = S_0\ (n\text{-independent}); \qquad S(n,t) = 0\ (\text{for } n = 0 \text{ and } N) \tag{11}$$

The relaxation modulus $G(t)$ of the probe chains is written in terms of $S(n,t)$ as[13-15,31]

$$G(t) = \frac{G_0}{NS_0}\int_0^N S(n,t)\,dn \tag{12}$$

where G_0 is the plateau modulus for the probe chains. (G_0 is proportional to c_{probe}/M_e, with M_e and c_{probe} being the entanglement spacing and probe concentration in mass/volume units, respectively.[1,2,13-15])

In the linear viscoelastic regime, all viscoelastic quantities are calculated from $G(t)$, and the decay of $G(t)$ is induced by an equilibrium thermal motion of the probe that also leads to slow dielectric relaxation (for type-A chains). Thus, we are observing the same motion through the dielectric and viscoelastic relaxation processes that are fundamentally described by $C(n,t;m)$ and $S(n,t)$, respectively. However, since C and S represent different (first and second) moments of the bond vector *at time t* (cf. eqs 1 and 10), the chain motion is differently reflected in these quantities. This fact can be easily confirmed, for example, from a comparison of viscoelastic loss moduli $G''(\omega)$ and dielectric loss factors $\epsilon''(\omega;0)$ (cf. eq 3) for Rouse and reptation mechanisms:[13,15] These mechanisms lead to the same $\omega\tau_1$ dependence of ϵ'' (τ_1 = longest relaxation time) but an entirely different dependence of G''. In other words, we can uniquely calculate G'' from ϵ'' (and vice versa) *only when* we know some details for the relaxation mechanism, e.g., for the cases of Rouse and/or reptation relaxation as well as for the case of relaxation of rigid spheres having dipoles and being imbedded in viscoelastic media as considered by DiMarzio and Bishop.[32]

To further examine a relationship between the viscoelastic and dielectric relaxation processes of type-A chains, we explicitly consider a change of the bond vector $\mathbf{u}$ in a short period of time between t and $t + \Delta t$. For adequately chosen Δt, we generally expect that the change is determined by the chain conformation at time t and described by an equation of the form

$$\mathbf{u}(n,t+\Delta t) = L^*(n;\Delta t)\,\mathbf{u}(n,t) + \Delta t(1/\zeta)\,\partial_n\,\mathbf{f}_B(n,t) \tag{13}$$

where $L^*(n;\Delta t)$ (=1 for $\Delta t = 0$) is an operator for $\mathbf{u}$ at time t, $\partial_n = \partial/\partial n$, ζ is the segmental friction, and $\mathbf{f}_B$ represents a random force characterized by relations $\langle\mathbf{f}_B(n,t)\rangle = 0$ and $\langle\mathbf{f}_B(n,t)\,\mathbf{f}_B(m,t')\rangle = Q\mathbf{I}\delta_{nm}\delta(t-t')$, with Q and $\mathbf{I}$ being the force intensity and unit tensor, respectively. The operation in eq 13, $L^*\mathbf{u}(n,t)$, may involve local operations (determined in the vicinity of n) like $(\partial_n)^2\,\mathbf{u}(n,t)$ and global operations like $\int_0^N h(n,n')\,\mathbf{u}(n',t)\,dn'$, with $h(n,n')$ being an integral kernel. The functional form of L^* changes with the features of chain motion: For example, for Rouse chains $L^* = 1 + \Delta t(\kappa/\zeta)\,\partial_n^2 + O(\Delta t^2)$, with κ being the spring constant, and for reptating chains with fixed contour length, $Q = 0$ and $L^* = 1 + (\xi/a)\,\partial_n + (\xi^2/2a^2)\,\partial_n^2 + O(\Delta t^2)$, with ξ being the segmental displacement along a tube during the period of time Δt. ($\langle\xi\rangle = 0$ and $\langle\xi^2\rangle \propto \Delta t$.)

Equation 13 leads to a time evolution equation (in a continuous limit) for a correlation function $S_2(n,m,t) = (1/a^2)\langle u_x(n,t)\,u_y(m,t)\rangle$,

$$\frac{\partial}{\partial t}S_2(n,m,t) = L_S(n,m)\,S_2(n,m,t) \tag{14}$$

where L_S is an operator defined by

$$L_S(n,m) = \left.\frac{\partial\langle L^*(n;\Delta t)\,L^*(m;\Delta t)\rangle}{\partial\Delta t}\right|_{\Delta t=0} \tag{15}$$

$S_2(n,m,t)$ is related to the orientation function $S(n,t)$ as

$$S_2(n,n,t) = S(n,t) \tag{16}$$

and satisfies the boundary and initial conditions

$$S_2(n,m,t) = 0 \text{ for } n,m = 0, N;\quad S_2(n,m,0) = S_0\delta_{nm} \tag{17}$$

Similarly, a time evolution equation for $C(n,t;m)$ is given by

$$\frac{\partial}{\partial t}C(n,t;m) = L_C(n)\,C(n,t;m) \tag{18}$$

where

$$L_C(n) = \left.\frac{\partial\langle L^*(n;\Delta t)\rangle}{\partial\Delta t}\right|_{\Delta t=0} \tag{19}$$

is an operator that determines the eigenfunctions f_p and eigenvalues $1/\tau_p$ involved in eq 4 as

$$L_C(n)\,f_p(n) = -(1/\tau_p)f_p(n) \tag{20}$$

(As for L^*, the operations $L_SS_2(n,m,t)$ (eq 14) and $L_CC(n,t;m)$ (eq 18) may involve local and global operations.)

As seen from eqs 15 and 19, the two operators L_S and L_C contain different moments of L^* so that the relationship between L_S and L_C is dependent on the features of L^*. (This fact can be easily confirmed again for Rouse and reptation mechanisms.) Namely, there is no general relationship between $S(n,t)$ and $C(n,t;m)$. However, for a special type of chain motion that induces *uncorrelated* changes of two bond vectors, we can find a rather simple relationship. For such motion, the operator $\langle L^*L^*\rangle$ involved in eq 15 can be decoupled as

$$\langle L^*(n;\Delta t)\,L^*(m;\Delta t)\rangle = \langle L^*(n;\Delta t)\rangle\langle L^*(m;\Delta t)\rangle + O(\Delta t^2) \tag{21}$$

so that L_S is related to L_C as (cf. eqs 15 and 19)

$$L_S(n,m) = L_C(n) + L_C(m) \quad (22)$$

Then, from eqs 14 and 18 together with the boundary and initial conditions (eqs 5, 6, and 17), $S(n,t)$ can be expanded with respect to f_p and τ_p defined for $C(n,t;m)$,

$$S(n,t) = S_0\frac{2}{N}\sum_{p=1}^{N}[f_p(n)]^2 \exp(-2t/\tau_p) \quad (23)$$

Furthermore, from eqs 12 and 23 and the Doi–Edwards expression for the plateau modulus, $G_0 = 4c_{probe}RT/5M_e$ (R = gas constant),[13-15] the ω dependence of dynamic moduli of the probe, $G^*_{probe} = G'_{probe} + iG''_{probe}$ ($i = (-1)^{1/2}$), is written in a reduced form,

$$\frac{G^*_{probe}M_{probe}}{c_{probe}RT} = \frac{8}{5}\sum_{p=1}^{N}[\int_0^1 f_p^2\, d(n/N)]\frac{ir_p\omega\tau^*}{1+ir_p\omega\tau^*}, \quad r_p = \tau_p/\tau^* \quad (24)$$

Here, τ^* is a relaxation time characterizing the terminal relaxation of the probe chain: τ^* can be the *longest viscoelastic relaxation time* ($=\tau_1/2$ when eq 23 is valid) or the *weight-average relaxation time* τ_w defined as the product of viscosity and compliance of the probe chain.[1-6] If eqs 21 and 22 are valid for the probe motion for various M_{probe} and M_{mat}, eq 24 gives a universal relationship between $G^*_{probe}M_{probe}/c_{probe}RT$ and $\omega\tau^*$ that is independent of those M's.

As seen from eq 24, viscoelastic quantities can be directly evaluated, *without assuming any molecular model*, from dielectrically obtained f_p and τ_p (and vice versa) for randomly moving chains characterized by eqs 21 and 22. In other words, *we can examine randomness of chain motion by testing the validity of eq 24*, as demonstrated in a later section. Concerning this fact, it should be noted that eq 24 never holds for coherently moving chains that do not satisfy eq 21. In particular, for chains of extremely coherent motion (like reptation) characterized by a relation,

$$\langle L^*(n;\Delta t)\, L^*(m;\Delta t)\rangle S_2(n,m,t)|_{n=m} = \langle L^*(n;\Delta t)\rangle S_2(n,n,t) + O(\Delta t^2) \quad (25)$$

we find, instead of eq 24,

$$G''(\omega)/G_0 = \epsilon''(\omega;0)/\Delta\epsilon \text{ (for type-A probe chains without dipole inversion)} \quad (26)$$

III. Experimental Section

III-1. Materials. Table 1 summarizes molecular characteristics of the probe PI and matrix polybutadiene (PB) chains. The PI chains are composed of two PI blocks (precursors) connected in a head-to-head fashion. The direction of dipoles is the same in each block but is inverted at the junction between the two blocks. The sample code numbers for those PI chains indicate molecular weights of the two blocks in units of 1000. As seen in Table 1, the PI chains have nearly the same M(≃48K) but differently inverted dipoles that are specified by the reduced location of the inversion point, n^*/N (cf. Figure 1).

All samples were synthesized and fully characterized in our previous work.[12,20,21] The B-9 sample was anionically synthesized in benzene with *sec*-butyllithium (s-BuLi).[12] The I-I 49-0 sample with dipole inversion at the end (i.e., without inversion) was synthesized in heptane with s-BuLi,[21] and the I-I 24-24 sample with *symmetrical* inversion at the chain center, by one-step coupling of PI anions with a prescribed amount of *p*-xylylene dichloride (XDC).[20] The other PI samples with *asymmetrically* inverted dipoles were synthesized by a *multistep* coupling method.[21] With this method, the end-chlorinated PI-Cl precursor of molecular weight M_1 ($>M/2$) was first made by single-chain termination of PI anions with a large amount of XDC, then excess XDC was removed by precipitation/redissolution procedures under vacuum, and finally living PI anions of molecular weight M_2 ($=M - M_1$) were coupled with the PI-Cl precursor.

Table 1. Characteristics of PI and PB Samples

code	$10^{-3}M$[a]	M_w/M_n	n^*/N[b]	precursor mol wt[c] $10^{-3}M_1$[a]	$10^{-3}M_2$[a]
Dipole-Inverted Probe PI[d]					
I-I 49-0[f]	48.8	1.05	0	48.8	
I-I 50-6	55.4	1.06	0.109	49.9	6.12
I-I 35-9	44.4	1.05	0.213	35.0	9.48
I-I 35-14	47.6	1.07	0.283	34.7	13.7
I-I 33-16	48.9	1.07	0.325	32.6	15.7
I-I 28-18	47.4	1.06	0.396	27.5	18.0
I-I 24-24[g]	47.7	1.06	0.5	23.9	
Matrix PB[e]					
B-9	9.24	1.07			

[a] Weight-average molecular weight. [b] Reduced location of the dipole inversion point. [c] $M_w/M_n \le 1.08$ for all precursor PI's. [d] cis:trans:vinyl ≃ 75:20:5. [e] cis:trans:vinyl ≃ 40:50:10. [f] Without dipole inversion. [g] With symmetrically inverted dipoles.

III-2. Measurements. Dielectric loss factors ϵ'' were measured at $25 \le T$ (°C) ≤ 80 with capacitance bridges (GR 1615A, General Radio; Precision LCR-meter 4284A, Hewlett-Packard) for *homogeneous* blends of the probe PI chains in the B-9 matrix. The B-9 matrix had negligibly small ϵ'' ($<10^{-4}$) at frequencies (ω) examined, and ϵ'' of the blends were attributed to fluctuation of the parallel dipoles of the probe PI due to its global motion. (Dipole components perpendicular to the PI chain contour have a negligibly small contribution to ϵ'' at those ω.)

For most cases, the PI content in the blend was ϕ_{PI} = 5 vol %. For the I-I 49-0/B-9 blend, we changed ϕ_{PI} and compared the reduced ϵ''/ϕ_{PI} curves for ϕ_{PI} = 3 and 5 vol %. These curves were identical, indicating that all PI probes (of almost identical M) were dilute and entangled only with the B-9 matrix in the blends with ϕ_{PI} = 5 vol %. (The entanglement between the probe and B-9 matrix was confirmed from the fact that the probe relaxation is 4–5 times slower in the B-9 matrix than in nonentangling, shorter PB matrices at an isofriction state.[33])

The time–temperature superposition worked very well for the PI/B-9 blends, and the ϵ'' data were reduced at T_r = 40 °C. At temperatures examined, the shift factor a_T was in a rather narrow range, $-1 < \log a_T < 0.5$, and ambiguities of the shift were negligibly small. Those a_T for the PI chains were identical to a_T for the B-9 matrix (determined from viscoelastic measurements), as found previously.[12] This result indicates that the segmental friction for the dilute PI chains uniformly mixed in the matrix is determined by local (segmental) motion of the matrix chains.

IV. Results

IV-1. Dielectric Loss Curves. Figures 2 and 3 compare the ϵ'' curves at 40 °C for homogeneous blends of the dipole-inverted PI chains (ϕ_{PI} = 5 vol %) in the matrix B-9 chains. As explained earlier, ϵ'' of the blends are attributed to the global motion of the dilute probe PI entangled with the matrix. In Figure 2, respective ϵ'' curves of the blends (unfilled symbols) are shifted vertically to avoid heavy overlapping of the data points, and in Figure 3 no vertical shifts are made so that differences of the curves can be most clearly observed. Figure 2 also shows the ϵ'' curves of the PI probes in their monodisperse bulk state[21] (filled symbols). These bulk curves are shifted to achieve the best superposition on the blend curves so that their shape is most clearly compared.

For the PI chains having slightly different molecular weights (cf. Table 1), the longest relaxation time τ_1 for the local correlation function (eq 4) is not exactly the same. Throughout this section (including Figures 2 and 3), we have corrected the small differences of τ_1 by shifting the

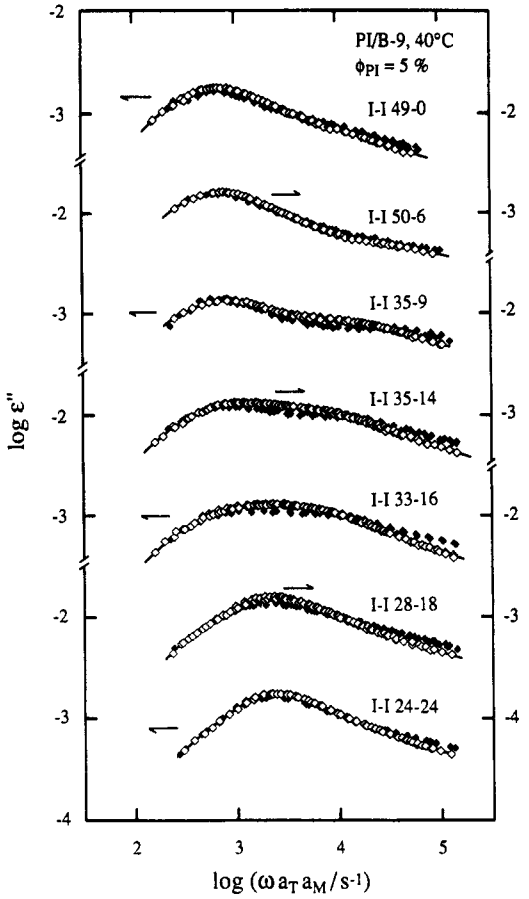

Figure 2. Frequency (ω) dependence of the dielectric loss factors ϵ'' at 40 °C for the dipole-inverted probe PI chains in the B-9 matrix (unfilled symbols). Small differences of their longest relaxation times τ_1 were corrected by shifts of the ϵ'' curves along the ω axis by factors a_M (Table 2). Respective curves were further shifted vertically to avoid heavy overlapping of the data points. For comparison, the curves for the PI chains in monodisperse bulk states[21] are adequately shifted and indicated with the filled symbols.

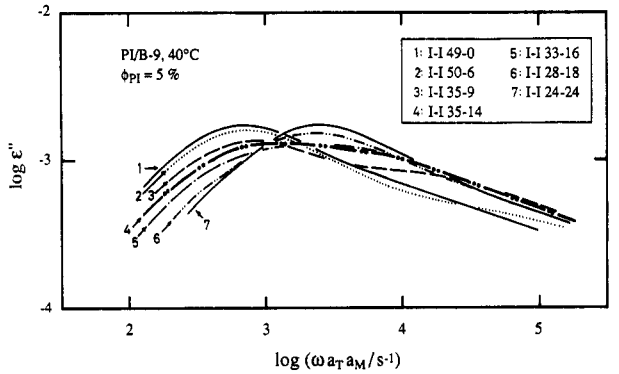

Figure 3. Comparison of the ϵ'' curves for the dipole-inverted PI probes in the B-9 matrix. Only the curves smoothly connecting the data points are shown, and no vertical shifts are made. As done in Figure 2, corrections for the small differences of τ_1 were made by the horizontal shifts.

ϵ'' curve of each blend along the ω axis by a factor $a_M = \tau_1/\tau_r$, with τ_r being τ_1 for the I-I 24-24/B-9 blend chosen as a reference for the shift. For evaluation of a_M, we interpolated the τ_1 data[12,33] of Figure 4 (large circles) obtained for various probe PI chains entangled with the B-9 matrix. The log a_M values are summarized in Table 2.

After the small correction for τ_1 ($|\log a_M| < 0.14$), we can consider the motion of the dipole-inverted PI chains in the blends to be exactly the same. Nevertheless, their ϵ''

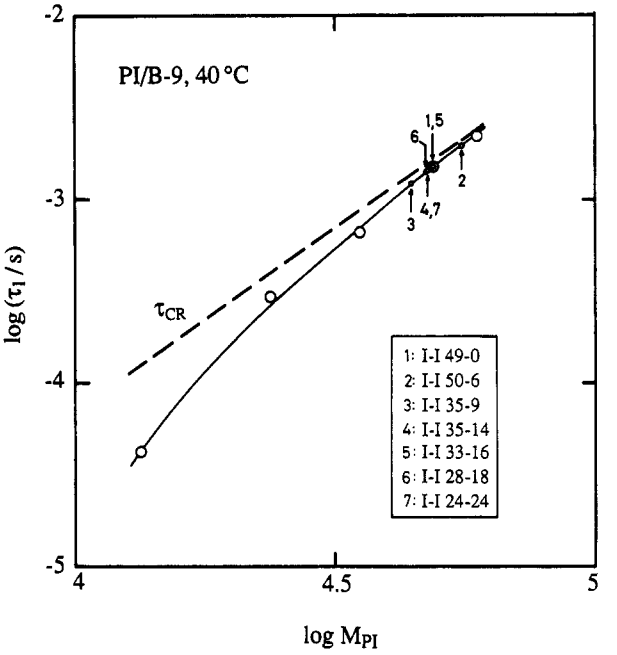

Figure 4. M_{PI} dependence of the longest relaxation time τ_1 at 40 °C for dilute PI chains entangled with the B-9 matrix[12,33] (large circles). Those PI chains had no inversion of dipoles, and τ_1 were evaluated from their ϵ'' peak frequencies. τ_1 for the dipole-inverted probe PI chains used in this study (small circles) were evaluated from interpolation. The dashed line indicates the constraint-release time experimentally obtained in ref 12.

Table 2. Correction Factors for Differences of τ_1 for the Probe PI Chains in the B-9 Matrix

probe PI	log a_M[a]	probe PI	log a_M[a]
I-I 49-0	0.021	I-I 33-16	0.023
I-I 50-6	0.135	I-I 28-18	−0.006
I-I 35-9	−0.070	I-I 24-24	0
I-I 35-14	−0.002		

[a] Evaluated from the τ_1 data shown in Figure 4.

curves shown in Figures 2 and 3 are quite different because of the differently inverted dipoles. As the dipole inversion point shifts from the chain end (I-I 49-0) to the center (I-I 24-24), the dielectric mode distribution observed as the shape of the curves first becomes broad and bimodal and then becomes narrow again. As discussed later, these changes provide detailed information for probe motion in the blend.

As seen from eqs 8 and 9, only odd eigenmodes of $C(n,t;m)$ contribute to ϵ'' of I-I 49-0 (with $n^* = 0$), while only even modes contribute to ϵ'' of I-I 24-24 (with $n^* = N/2$). Thus, the terminal relaxation times *dielectrically observed* for the I-I 49-0/B-9 and I-I 24-24/B-9 blends are τ_1 and τ_2 for the first and second eigenmodes, respectively. In Figure 5, the ϵ'' curve of the former is shifted along the ω axis by a factor $\Delta_M = 3.6$ and compared with the curve of the latter. The two curves are indistinguishable, meaning that the relaxation mode distribution is the same for the I-I 49-0 and 24-24 chains and $\tau_2 = \tau_1/3.6$. Specifically, the τ_1 and τ_2 values are evaluated from their ϵ'' peak frequencies as

$$\tau_1 = 1.62 \times 10^{-3}\ \text{s}, \quad \tau_2 = 0.45 \times 10^{-3}\ \text{s} \qquad (27)$$

Here, we return to Figure 2 and compare the ϵ'' curves for the blends (unfilled symbols) and monodisperse bulk systems (filled symbols). For the PI chains with dipole inversion at $n^*/N \cong 0$ and $^1/_2$, the dielectric mode distribution seen as the shape of the curves is almost the same in the two environments. In particular, for $n^*/N =$

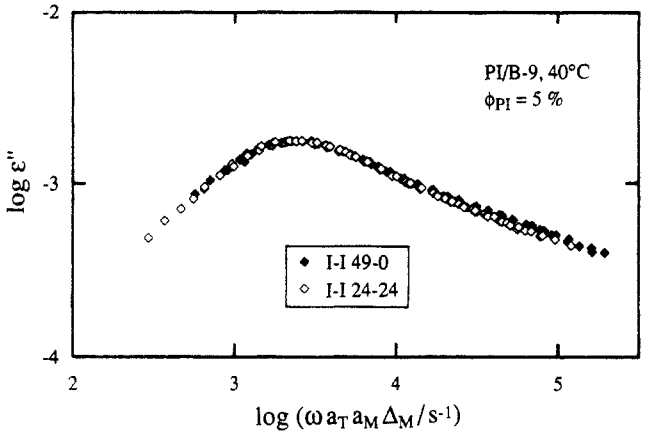

Figure 5. Comparison of the ϵ'' curves at 40 °C for the I-I 49-0 and I-I 24-24 chains in the B-9 matrix. The curve for the former is shifted along the ω axis first by a factor $a_M = 1.05$ (a correction for the difference of τ_1) and further by a factor $\Delta_M = 3.6$.

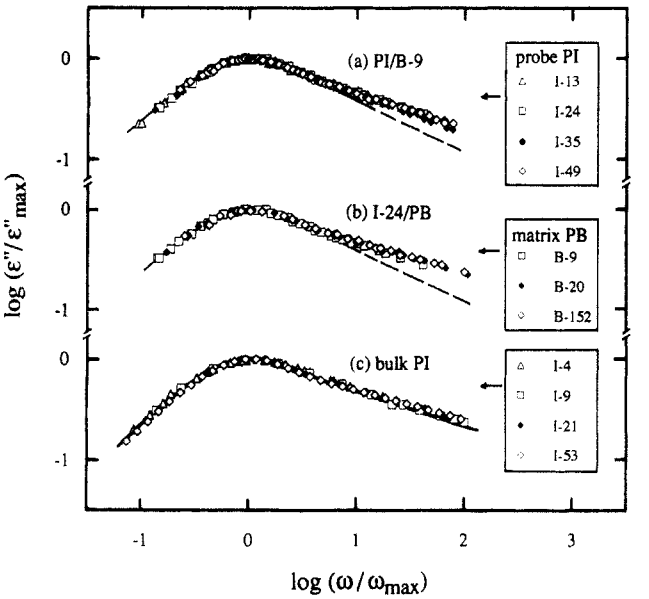

Figure 6. ϵ'' curves reduced at peaks for PI chains without dipole inversion.[12,24,25] Comparison is made for (a) different probe PI chains in the same B-9 matrix, (b) the same probe PI chain in different PB matrices, and (c) various PI chains in their monodisperse bulk state. The sample code numbers indicates the molecular weights in units of 1000. Note that the PI chains examined in part c have molecular weights below and above the characteristic M_c for entanglement (M_c = 10K for bulk PI[1,2]). The dashed curves in parts a and b indicate the ϵ'' curves calculated by the Rouse CR model with a correction for small molecular weight distribution.[12] The blend data of parts a and b are shown in part c with the solid curve.

0, the mode distribution is quite insensitive to M_{probe}, M_{mat}, and even the existence of entanglement,[34,35] as demonstrated in Figure 6 where the ϵ'' curves[12,24,25] are compared at low ω for (a) different probe PI chains in the same PB (B-9) matrix, (b) the same probe in different matrices, and (c) monodisperse bulk PI of molecular weights above and below the characteristic M_c for entanglement (=10K for bulk PI[1,2]). The monodisperse systems (part c) are classified as special blends with $M_{probe} = M_{mat}$, and their mode distribution is very close to that of the blends (solid curve in part c).

In contrast to the above results for $n^*/N \cong 0$ and $^1/_2$, the blends and bulk systems with $n^*/N \cong {}^1/_4$ exhibit non-negligible differences of the shape of ϵ'' curves at intermediate to high ω (cf. Figure 2). These differences may correspond to differences of the probe motion in these systems, as discussed in a later section.

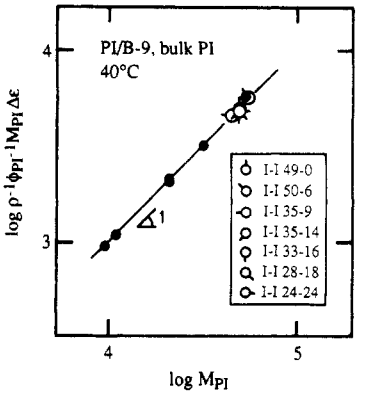

Figure 7. Plots of reduced dielectric relaxation intensities, $\Delta\epsilon^* = \rho^{-1}\phi_{PI}^{-1}M_{PI}\Delta\epsilon$ ($\propto \langle R_e^2 \rangle$), against M_{PI} for the dipole-inverted PI probes in the B-9 matrix (unfilled circles). For comparison, $\Delta\epsilon^*$ are shown also for monodisperse bulk PI[12,24,25] (filled circles).

IV-2. Relaxation Intensity. For the probe PI chain of molecular weight M_{PI}, the dielectric intensity $\Delta\epsilon$ for the global relaxation (cf. eq 3) is related to the mean-square end-to-end distance $\langle R_e^2 \rangle$ as[22,24]

$$\Delta\epsilon = \frac{4\pi\phi_{PI}\rho N_A \mu^2 F}{3kT}\frac{\langle R_e^2 \rangle}{M_{PI}} \tag{28}$$

Here, ρ is the density of the system; kT, the thermal energy; N_A, Avogadro's number, μ, the dipole moment per unit contour length; F(=constant close to unity in nonpolar environments), the ratio of internal to external electric field strength; and ϕ_{PI}, the PI content in the blend. We have evaluated $\Delta\epsilon$ for the dipole-inverted PI probes by integrating their ϵ'' data (Figure 2) with respect to ln ω[36] and examined the M_{PI} dependence of reduced intensities, $\Delta\epsilon^* = \rho^{-1}\phi_{PI}^{-1}M_{PI}\Delta\epsilon$. The results are shown in Figure 7 (unfilled symbols) together with $\Delta\epsilon^*$ for monodisperse bulk PI[12,24,25] (filled symbols). Clearly, $\Delta\epsilon^*$ for the probe PI chains in the B-9 matrix are proportional to M_{PI} and very close to $\Delta\epsilon^*$ for bulk PI. Since $\Delta\epsilon^*$ is proportional to $\langle R_e^2 \rangle$ (cf. eq 28), this result strongly suggests that the PI probes have a Gaussian conformation as bulk PI does. Thus, eq 9 derived for Gaussian chains is safely applied to those probes.

IV-3. Eigenfunctions for $C(n,t;m)$. Fitting the ϵ'' data with low-ω forms of eq 7,

$$\epsilon''(\omega;n^*) = g_1(n^*)\,D_1(\omega) + g_2(n^*)\,D_2(\omega) + G_3(n^*)\,\omega \tag{29}$$

and

$$\epsilon''(\omega;n^*) = g_1(n^*)\,D_1(\omega) + g_2(n^*)\,D_2(\omega) + g_3(n^*)\,D_3(\omega) + G_4(n^*)\omega \tag{30}$$

we can decompose the data into dielectric modes and further determine the eigenfunctions for $C(n,t;m)$. Here, $D_p(\omega) = \omega\tau_p/(1 + \omega^2\tau_p^2)$ is the single relaxation function for the pth mode, and $G_q(n^*)\omega$ (q = 3, 4) is the low-ω asymptote of the contribution $\epsilon_{(\geq q)}''$ from all kth modes with $k \geq q$,

$$\epsilon_{(\geq q)}'' = \sum_{k \geq q} g_k(n^*)\,D_k(\omega) \tag{31}$$

The τ_1 and τ_2 values specifying the location of $D_1(\omega)$ and $D_2(\omega)$ were already determined (eq 27), and the τ_3 value (=0.25 × 10^{-3} s) for $D_3(\omega)$ was evaluated from the ϵ'' data of I-I 49-0 by a linear least-squares fitting (LLSF) method explained previously.[21] Thus, eqs 29 and 30 are linear equations for unknown quantities, $g_1 - g_3$ (and G_3 and G_4),

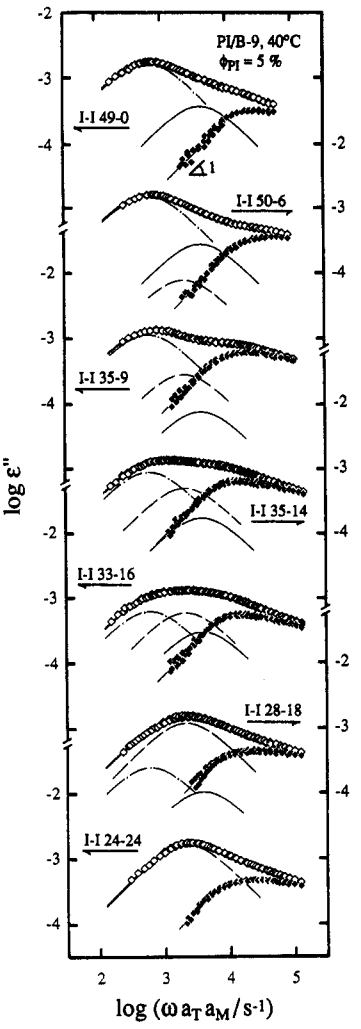

Figure 8. Results of the mode decomposition of the ϵ'' data (unfilled symbols) by the fit with eq 30 for the dipole-inverted PI chains in the B-9 matrix. The dash-dotted, dashed, and solid curves indicate the contributions from the first to third eigenmodes, $g_pD_p(\omega)$ with p = 1–3. The higher mode contribution, $\epsilon_{(\geq 4)}''$ (eq 31), is indicated with the filled symbols. The thick solid curves indicate the recalculated $\epsilon'' = g_1D_1 + g_2D_2 + g_3D_3 + \epsilon_{(\geq 4)}''$, with $\epsilon_{(\geq 4)}''$ being evaluated for the thin curves that smoothly connect the filled symbols.

so that these quantities can be determined, with the highest accuracy attainable, from standard LLSF of the ϵ'' data at low ω with eqs 29 and 30. Details of fitting procedures were described previously.[21]

Figure 8 demonstrates the results of the fit with eq 30. The ϵ'' data are shown with the unfilled symbols, and the first to third mode contributions, g_1D_1, g_2D_2, and g_3D_3, are indicated with the thin dash-dotted, dashed, and solid curves, respectively. The filled symbols represent the higher mode contribution, $\epsilon_{(\geq 4)}'' = \epsilon'' - g_1D_1 - g_2D_2 - g_3D_3$. We see that the prerequisite of the fit, $\epsilon_{(\geq 4)}'' \propto \omega$, is well satisfied at low ω and the mode decomposition is well achieved. A similar quality of fit was obtained also for eq 29, and the g_1 and g_2 values determined from the fit with eq 29 were very close to those with eq 30.

Using those $g_1 - g_3$ and $\Delta\epsilon$ (cf. Figure 7) in eq 9, we evaluated the integrated eigenfunctions $F_p(n^*)$ (p = 1–3). Figure 9 shows $\Delta F_p(n^*) = F_p(n^*) - F_p(N/2)$ (p = 1–3) for the PI chains in the B-9 matrix (unfilled circles) and in their monodisperse bulk state[21] (filled squares). We note that $\Delta F_p(n^*)$ are nearly the same in these environments. For the PI chains in the B-9 matrix, the eigenfunctions $f_p(n) = [N/2^{1/2}][d\Delta F_p(n)/dn]$ (cf. eq 8) were evaluated as an average gradient (in an interval of $\Delta(n/N) = 0.1$) taken

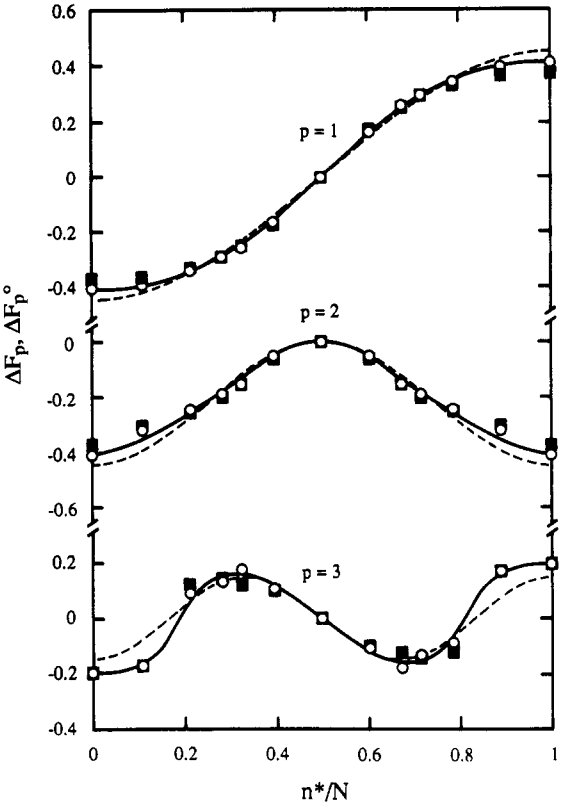

Figure 9. Plots of integrated eigenfunctions, $\Delta F_p(n^*) = F_p(n^*) - F_p(N/2)$ (p = 1–3), against n^*/N for probe PI chains in the B-9 matrix (unfilled circles). For comparison, $\Delta F_p(n^*)$ for monodisperse bulk PI[21] are shown with the filled squares. The dashed curves indicate $\Delta F_p°(n^*) = [2^{1/2}/p\pi][\cos(p\pi/2) - \cos(p\pi n^*/N)]$ predicted from the Rouse CR model. Note that ΔF_p and $\Delta F_p°$ are normalized according to eq 6.

for the solid curves that smoothly connect the ΔF_p data points. The results are shown in Figure 10.

Most of molecular models so far proposed (including those explained in the next section) have *sinusoidal* eigenfunctions for $C(n,t;m)$,

$$f_p°(n) = \sin(p\pi n/N) \tag{32a}$$

and

$$\Delta F_p°(n^*) = (2^{1/2}/p\pi)[\cos(p\pi/2) - \cos(p\pi n^*/N)] \tag{32b}$$

These model functions (normalized according to eq 6) are shown in Figures 9 and 10 with the dashed curves. As seen in Figure 9, the experimental ΔF_p (symbols) are fairly close to the model $\Delta F_p°$ for $n^* \cong N/2$ but systematically deviate from $\Delta F_p°$ as n^* approaches 0 or N, and the differences between ΔF_p and $\Delta F_p°$ at $n^* = 0$ and N are larger than the uncertainties in evaluation of ΔF_p. Correspondingly, we see in Figure 10 that $|f_p|$ becomes smaller than $|f_p°|$ (in particular for p = 1 and 3) as n approaches 0 and N. These results of Figures 9 and 10 demonstrate the *nonsinusoidal* n dependence of the experimental $f_p(n)$ and $\Delta F_p(n)$ obtained for the PI probes in the blends, although deviations from the sinusoidal $f_p°$ and $\Delta F_p°$ are not extremely large.

The nonsinusoidal f_p and ΔF_p may indicate coupling of pure Rouse modes (having sinusoidal $f_p°$ and $\Delta F_p°$). Fourier analyses on f_p and ΔF_p can provide the coupling coefficients, and the results will be presented in our future paper for PI chains in various environments (including the blends examined here).

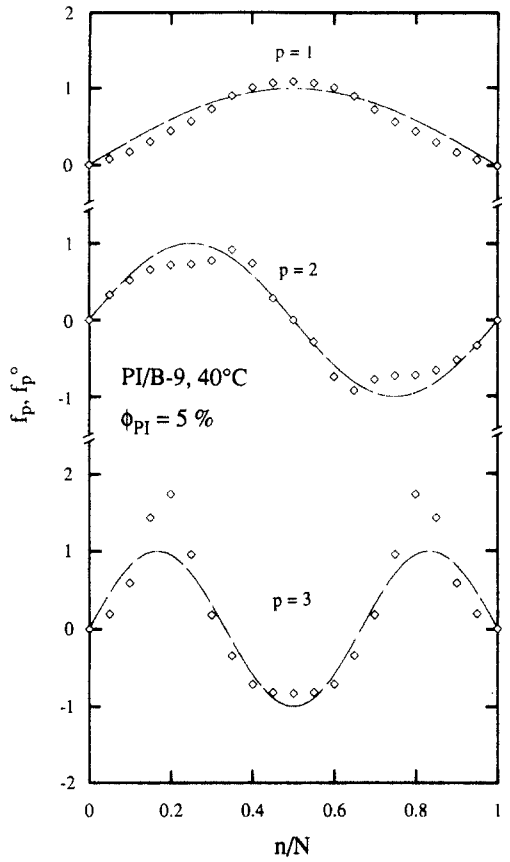

Figure 10. Eigenfunctions $f_p(n)$ for the probe PI chains in the B-9 matrix (symbols) evaluated from the ΔF_p data shown in Figure 9. The dashed curves indicate $f_p^\circ(n) = \sin(p\pi n/N)$ predicted from the Rouse CR model. Note that f_p and f_p° are normalized according to eq 6.

V. Discussion

V-1. CR Effect on Eigenmodes. As explained earlier, the probe relaxation behavior in blends is dependent on the matrix and probe molecular weights M_{mat} and M_{probe}. For $M_{mat} \ll M_{probe}$, the probe relaxation is dominated by a *constraint-release* (CR) mechanism that is defined, *in a general sense*, as a mechanism for which the probe relaxes locally as the matrix rapidly diffuses away and globally by accumulating such local processes. We here examine whether this CR mechanism affects the eigenmodes for the local correlation function $C(n,t;m)$.

Data for the CR relaxation time τ_{CR} of probe chains entangled with *much shorter* matrices[3-6,12] can be summarized as[37]

$$\tau_{CR} = k_{CR} M_{probe}^{\ 2} M_{mat}^{\ 3} \qquad (33)$$

Using $k_{CR} = 8.94 \times 10^{-25}$ s (40 °C) previously determined for PI/PB blends,[12] we have evaluated τ_{CR} for PI chains in the B-9 matrix. The results have been shown in Figure 4 with the dashed line. As seen there, τ_1 for the dipole-inverted PI chains used in this study (small symbols) are close to τ_{CR}, indicating that the global relaxation of these PI chains in the B-9 matrix is dominated by the CR mechanism. On the other hand, $\tau_1 \cong \tau_{CR}/3.5$ for those PI chains (with $M \cong 48$K) in the monodisperse bulk state.[38] Thus, the CR contribution to the probe relaxation is much smaller in the monodisperse systems than in the B-9 blends. Nevertheless, in these environments, the PI chains have nearly the same ΔF_p (Figure 9) and τ_p ratio for the lowest three eigenmodes. ($\tau_1/\tau_2/\tau_3 \cong 1/0.28/0.15$ for the blends and $\cong 1/0.26/0.14$ for the monodisperse systems.[21]) In addition, for the PI chains with $n^* = 0$, the dielectric mode distribution is insensitive to M_{probe} and M_{mat} (cf. Figure 6). These facts strongly suggest that the distribution of the low-order eigenmodes of $C(n,t;m)$ is insensitive to the CR contribution.

However, in Figure 2, we have also found nonnegligible differences of the shape of the ϵ'' curves for the blends and bulk systems with $n^*/N \cong 1/4$. For $n^*/N \cong 1/4$, ϵ'' at intermediate ω has a magnified contribution from higher order eigenmodes (in particular from the fourth mode) and the differences may indicate some CR effect that is enhanced for the higher order modes. (For $n^*/N \cong 0$ and $1/2$, those modes do not largely contribute to ϵ'' and the CR effect, if any, is not clearly observed.) However, we remember that only the single-chain autocorrelation contributes to ϵ'' of the *dilute* PI chains in the blends (cf. eq 2), while an additional contribution from the interchain correlation might exist for bulk PI systems.[39] This additional contribution would be negligibly small *at low* ω where the ϵ'' curves have nearly the same shape in the blend and bulk (even for $n^*/N \cong 1/4$), but not necessarily *at high* ω. The differences found for $n^*/N \cong 1/4$ might be due also to the interchain correlation in bulk systems. Thus, as imporant future work, we need to examine the CR effect in the clearest fashion for *dilute* PI chains of various n^* in short and long matrices.

V-2. Details of CR Eigenmodes. In the remaining part of this paper, we focus our attention on the probe relaxation *in blends*. As seen in Figure 4, the relaxation of the dipole-inverted PI chains in the B-9 matrix is dominated by the CR mechanism that has a general feature, accumulation of local relaxation induced by the matrix motion. For this mechanism, conventional modified tube models further assume that the accumulation takes place in a *Rouse fashion*.[15-17] We here examine the validity and limitation of this Rouse CR model.

For the local correlation function $C(n,t;m)$ deduced from the model, the eigenfunctions f_p° are sinusoidal (eq 32), and the relaxation time is scaled as

$$\tau_p^\circ = \tau_1^\circ/p^2 \ (p = 1, 2, \ldots); \quad \tau_1^\circ = \tau_{CR}^\circ \propto M_{probe}^{\ 2} M_{mat}^{\ 3} \qquad (34)$$

This model prediction for the M_{probe} and M_{mat} dependence of τ_1 is in agreement with the data for probe chains entangled with much shorter matrices (eq 33). The prediction for the τ_p ratio for the lowest three eigenmodes, $\tau_1^\circ/\tau_2^\circ/\tau_3^\circ = 1/0.25/0.11$, is reasonably close to the ratio obtained for the probe PI chains in the B-9 blends, $\tau_1/\tau_2/\tau_3 \cong 1/0.28/0.15$. In addition, the coincidence of the shape of ϵ'' curves for $n^* = 0$ and $N/2$ (Figure 5) is deduced from the model, and the predicted shift factor $\Delta_M = 4$ is close to the observed $\Delta_M = 3.6$.

Despite these agreements, the Rouse CR model has a definite limitation. In parts a and b of Figure 6, the ϵ'' curve calculated by the model for the case of $n^* = 0$ is indicated with the dashed curve. Comparing this curve with the data in part a for the I-49/B-9 blend (that is in the CR regime), we note that the model underestimates the dielectric relaxation at high ω to predict smaller ϵ''. This disagreement suggests differences of higher order CR eigenmodes for the actual PI chains and the model, as pointed out in our previous work.[6,12]

Figure 11 shows the ϵ'' curves calculated by the Rouse CR model for the dipole-inverted PI chains. In the calculation, τ_1° and $\Delta\epsilon$ were adequately chosen so that the height and location of the ϵ'' peak were reproduced for the I-I 49-0 chain. Small distribution of M and n^* for the PI chains hardly changed the calculated ϵ'' curves.

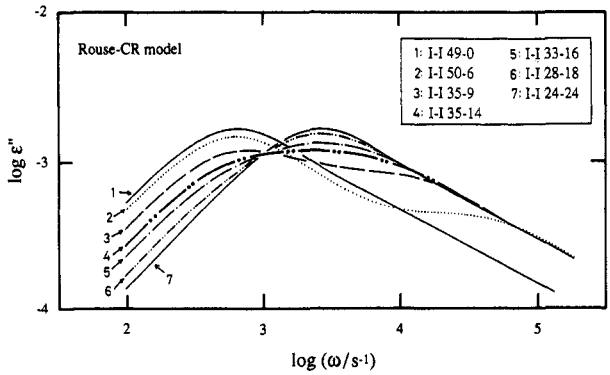

Figure 11. ϵ'' curves for the dipole-inverted PI chains calculated from the Rouse CR model. In the calculation, τ_1° and $\Delta\epsilon$ were adequately chosen so that the height and location of the ϵ'' peak were reproduced for the I-I 49-0 chain.

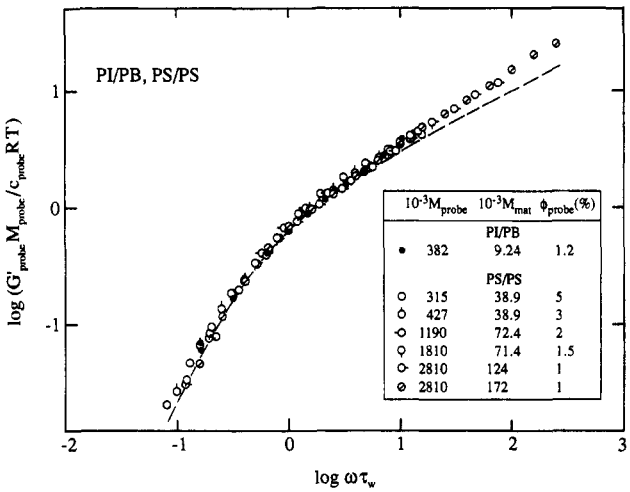

Figure 12. Plots of reduced modulus $G'_{probe}M_{probe}/c_{probe}RT$ against reduced frequency $\omega\tau_w$ for probe PI and PS chains entangled with much shorter matrix chains.[3-6,12] The short matrices had a negligibly small contribution to G'_{blend} of the blend at low ω examined here, and G'_{probe} of the probe chains were identical to G'_{blend}. The dashed curve indicates the prediction of the Rouse CR model with a correction for the small molecular weight distribution.[5]

Comparing Figures 3 and 11, we note that the model qualitatively describes changes of the ϵ'' curves with n^*. However, close inspection reveals quantitative differences between the observed and calculated curves *even at low* $\omega < 2 \times 10^3\ s^{-1}$ ($\cong 1/\tau_2$). (For example, compare the shape and peak location for curve 4 in the two figures.) Higher order modes with $p \geq 4$ have negligible contribution to ϵ'' at those low ω, as noted from a comparison of ϵ'' and $\epsilon_{(\geq 4)}''$ shown in Figure 8. Thus, the differences of ϵ'' at low ω are mainly due to the differences between the actual and Rouse CR eigenmodes with $p = 1$–3, specifically, the differences between f_p and f_p° (Figure 10).

As explained earlier, viscoelastic and dielectric relaxation processes differently reflect the global chain motion. Thus, for specifying the limitation of the Rouse CR model, it is also important to compare the model predictions with viscoelastic data in the CR regime, i.e., with the data for dilute probe chains entangled with *much shorter* matrices. We have extensively studied the behavior of such probe chains for polystyrene (PS) blends[3-6] and also for PI/PB blends.[12] Figure 12 demonstrates the representative data (symbols) and the prediction of the Rouse CR model (dashed curve), both in a reduced form suggested by eq 24, $G'_{probe}M_{probe}/c_{probe}RT$ *versus* $\omega\tau_w$. (Since the weight-average relaxation time τ_w is more accurately evaluated from the G^* data than the longest viscoelastic relaxation

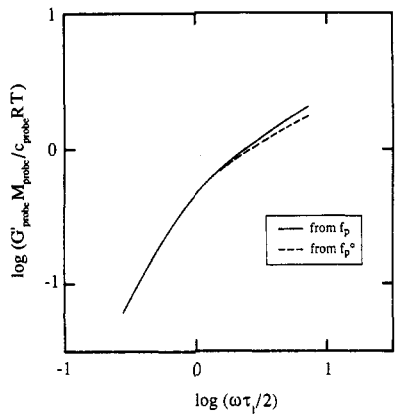

Figure 13. Dependence of reduced modulus $G'_{probe}M_{probe}/c_{probe}RT$ evaluated from dielectrically determined f_p and τ_p ($p = 1$–3) on reduced frequency $\omega\tau_1/2$ (solid curve). The longest viscoelastic relaxation time $\tau_1/2$ is a little longer than the weight-average relaxation time τ_w used in Figure 12. The dashed curve indicates the reduced modulus calculated from f_p° and τ_p° ($p = 1$–3) of the Rouse CR model.

time $\tau_1/2$, we have used τ_w in Figure 12 as the characteristic time involved in the reduced frequency.)

In Figure 12, we first note that the data for various probe chains are collapsed into a universal curve. This universality indicates that the actual CR mechanism has a random nature specified by eqs 21 and 22, as is the case also for the Rouse CR mechanism. Concerning this result, we note that the universal curve is very close to the model prediction at low ω. However, with increasing ω, the data systematically deviate upward from the prediction, as pointed out previously.[5,6] Thus, the Rouse CR model *overestimates* viscoelastic relaxation at intermediate to high ω to predict smaller G'. This result is in contrast to the *underestimation* for the dielectric relaxation seen in Figure 6.

As explained above, eqs 21 and 22 hold for the actual CR mechanism. For this case, we should be able to use eq 24 and evaluate the reduced modulus $G'_{probe}M_{probe}/c_{probe}RT$ from the dielectrically determined f_p (Figure 10) and τ_p. The solid curve in Figure 13 indicates the dependence of the modulus obtained from f_p and τ_p with $p = 1$–3 on the reduced frequency $\omega\tau_1/2$. ($\tau_1/2$ is a little longer than τ_w.) For comparison, the modulus calculated from the lowest three Rouse CR modes is indicated with the dashed curve. The *dielectrically evaluated* modulus is close to the model prediction at low ω but systematically deviates upward with increasing ω.

All eigenmodes are involved in the data and the model prediction shown in Figure 12, while only the lowest three eigenmodes are used in the evaluation of the moduli shown in Figure 13. Thus, we cannot compare Figures 12 and 13 in a very quantitative way. Nevertheless, we note considerable agreement between the viscoelastic data and the dielectrically evaluated modulus (symbols in Figure 12 and the solid curve in Figure 13). This agreement means that the dielectric and viscoelastic relaxation processes of the probe chains are consistently described by a non-Rouse-type CR mechanism. In other words, the under- and overestimation of the Rouse CR model for these processes (cf. Figures 6 and 12) are a natural consequence of the non-Rouse nature of the actual CR mechanism.

V-3. Origin of Non-Rouse Nature of CR Relaxation. As discussed in the previous section, detailed features of the actual CR mechanism are not described by the Rouse CR model.[40] For further discussion of the non-Rouse nature of the actual mechanism, it is useful to reexamine how the Rouse nature is introduced in the model. The

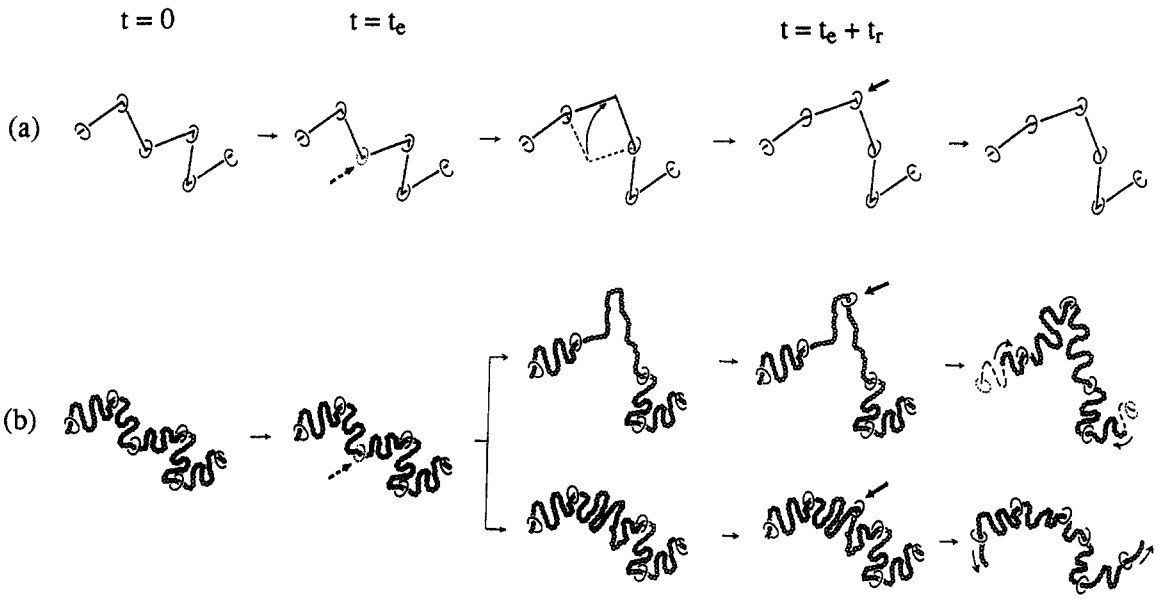

Figure 14. (a) Schematic illustration of local CR motion for a Verdier–Orwell–Stockmayer (VOS) chain used in the Rouse CR model and (b) possible local motion considered for a real probe chain. A link is destroyed at $t = t_e$ and reconstructed at $t = t_e + t_r$, as indicated with the thick dashed and solid arrows. The beads drawn in part b schematically indicate the monomers of the probe chain. Note that the contour length is preserved during the local CR jump for the VOS chain but not necessarily for the real chain.

fundamental motion of a probe chain considered in the model is depicted in part a of Figure 14.

In the Rouse CR model,[15] a real probe chain is replaced by a Verdier–Orwoll–Stockmayer (VOS) chain[41] composed of N rods. Each rod corresponds to an entanglement segment composed of n_e monomers, and the rod length is fixed at an equilibrium entanglement length a. Junctions between the rods are constrained by entangling matrix chains, as depicted by the slip links in Figure 14. Each link has an average lifetime t_e and is destroyed when one of entangling matrix chains diffuses away. The destroyed link is reconstructed (not necessarily at the same point in space) as some matrix chain approaches the released junction. This reconstruction should take some time t_r (that is determined by the matrix motion). Thus, on average, a link formed at $t = 0$ is destroyed at $t = t_e$ and reconstructed at $t = t_e + t_r$, as indicated with the thick dashed and solid arrows in part a of Figure 14. In the period of time $t_e < t < t_e + t_r$, the released junction is allowed to move in a flip–flop fashion according to some stochastic jump rule. During this process, the VOS chain locally relaxes but its contour length is preserved. Irrespective of the details of the jump rule, accumulation of those local, uncorrelated jumps leads to a Rouse-like global relaxation.

One possible local motion of the real probe chain trapped in an array of slip links is considered in part b of Figure 14. For $0 < t < t_e$, all links are preserved and the n_e monomers (shown as the beads) involved in each entanglement segment would move as a flexible strand that is constrained at the links. At $t = t_e$, a link is destroyed and the two strands separated by this link at $t < t_e$ are merged into a larger strand (composed of $2n_e$ monomers). Then, large-scale motion of this new strand frozen by the link at $t < t_e$ is activated. During this motion ($t_e < t < t_e + t_r$), an end-to-center distance of the new, enlarged strand need not be preserved for the real probe chain, as is different from the situation for the VOS chain. In other words, this strand may take various conformations that involve elongated, hairpin-like conformations as well as shrunk conformations. When the link is reconstructed at $t = t_e + t_r$, the enlarged strand still keeps its shape but is divided into two shorter strands, each having n_e monomers on average. The end-to-end distances of these two strands are not necessarily identical to the equilibrium distances, and the tension along the chain contour may be unbalanced at these strands. Then, longitudinal motion of the probe chain would be induced to recover the tension balance, either sucking in or pushing out some monomers along the array of the links, as shown in part b of Figure 14. (This tension equilibration process is somewhat similar to the contour length fluctuation process considered in modified tube models,[13–15] but we should note an important difference that the former is activated by the matrix motion while the latter is irrelevant to this motion.) Finally, rearrangements of links along the chain contour may take place to recover an equilibrium entanglement density.

As seen from part b of Figure 14, the length-variable local jump may provide some extra relaxation at chain ends that is not considered in the Rouse CR model. As discussed previously,[21] analogies between the eigenfunction equation for $C(n,t;m)$ and the Schrödinger equation indicate that the extra relaxation source at chain ends tends to distort the eigenfunction from the sinusoidal $f_p°$ toward the observed f_p. Thus, the length-variable local jump is one possible motion that provides the non-Rouse nature to the actual CR mechanism, and it is interesting to formulate a CR model for this motion. However, we emphasize that this jump is not the *only* possible motion providing the extra relaxation at chain ends and examination of other possible motion is also important.

V-4. Problems of Modified Tube Models. Conventional modified tube models assume reptation for the relaxation of probe chains in much longer matrices ($M_{mat} \gg M_{probe}$). The reptation model has sinusoidal $f_p°$ (eq 32) and p^{-2} dependence of τ_p. Thus, this model predicts the dielectric relaxation mode distribution being identical to that for the Rouse CR model, as indicated with the dashed curve in part b of Figure 6. As seen there, the ϵ'' curve of the I-24 chain in the *much longer* PB-152 matrix is broader than the reptation prediction, suggesting that the actual eigenmodes have nonsinusoidal (nonreptative) f_p even for $M_{mat} \gg M_{probe}$. Such nonreptative nature may result from some mechanism providing extra relaxation at chain ends, but not from the length-variable local jump *induced by the matrix motion* (Figure 14b). In relation to this result,

we remember that eq 26 does not hold even for highly entangled monodisperse PI chains.[26] Namely, those chains do not move in the extremely coherent fashion specified by eq 25. Further study is desired for the chain motion in highly entangled systems.

For general cases of arbitrary M_{mat} and M_{probe}, the probe relaxation is determined by competition of two asymptotic mechanisms that dominate the behavior at low-M_{mat} and high-M_{mat} limits. For dielectric and viscoelastic relaxation processes, this competition should be formulated for the fundamental local functions, $C(n,t;m)$ (eq 1) and $S(n,t)$ (eq 10), not for the relaxation functions $\Phi(t)$ (eq 2) and $G(t)$ (eq 12) obtained as the averages of C and S. Watanabe and Tirrell considered this fact and formulated a configuration-dependent CR (CDCR) model[12,17] for the competition of the Rouse CR and reptation mechanisms. As extensively examined in our previous work,[5,6,12] this model considerably well describes the M_{probe} and M_{mat} dependence of both dielectric and viscoelastic relaxation times, the M_{probe} and M_{mat} independence of the dielectric mode distribution (cf. Figure 6), and changes of the viscoelastic mode distribution with M_{probe} and M_{mat}. Nevertheless, the Rouse CR and reptation mechanisms involved in the CDCR model do not describe details of probe relaxation, as discussed in this paper. Thus, in a refined model, competition should be considered for actual asymptotic mechanisms to formulate time evolution equations for $C(n,t;m)$ and $S(n,t)$. This refinement is interesting future work.

VI. Concluding Remarks

The dielectric study on the dipole-inverted PI chains in the short B-9 matrix has revealed the non-Rouse nature of the actual CR relaxation that is most clearly observed for the nonsinusoidal n dependence of the eigenfunctions (Figures 9 and 10). Considerable agreements are found for the viscoelastically and dielectrically determined moduli of long probe chains in much shorter matrices (Figures 12 and 13), indicating that the under- and overestimation of the Rouse CR model for the dielectric and viscoelastic relaxation processes (Figures 6 and 12) are a natural consequence of the non-Rouse nature of the actual CR mechanism and that the probe chain locally moves in a random fashion as specified by eqs 21 and 22. These detailed experimental facts would provide a clue for further studying the origins of the non-Rouse nature of the actual CR mechanism and also for formulating a refined model that is applicable in an entire range of M_{probe} and M_{mat}.

References and Notes

(1) Ferry, J. D. *Viscoelastic Properties of Polymers*, 3rd ed.; Wiley: New York, 1980.
(2) Graessley, W. W. *Adv. Polym. Sci.* **1974**, *16*, 38.
(3) Watanabe, H.; Sakamoto, T.; Kotaka, T. *Macromolecules* **1985**, *18*, 1436.
(4) Watanabe, H.; Kotaka, T. *Macromolecules* **1986**, *19*, 2520; **1987**, *20*, 530.
(5) Watanabe, H.; Yamazaki, M.; Yoshida, H.; Kotaka, T. *Macromolecules* **1991**, *24*, 5573.
(6) Watanabe, H.; Kotaka, T. *Chemtracts: Macromol. Chem.* **1991**, *2*, 139 and references therein.
(7) Montfort, J.-P., Marin, G.; Monge, P. *Macromolecules* **1984**, *17*, 1551; **1986**, *19*, 1979.
(8) Green, P. F.; Mills, P. J.; Palmstrøm, C. J.; Mayer, J. W.; Kramer, E. J. *Phys. Rev. Lett.* **1984**, *53*, 2145. Green, P. F.; Kramer, E. J. *Macromolecules* **1986**, *19*, 1108.
(9) Antonietti, M.; Coutandin, J.; Sillescu, H. *Macromolecules* **1986**, *19*, 793.
(10) Nemoto, N.; Kojima, T.; Inoue, T.; Kishine, M.; Hirayama, T.; Kurata, M. *Macromolecules* **1989**, *22*, 3793. Nemoto, N.; Kishine, M.; Inoue, T.; Osaki, K. *Macromolecules* **1990**, *23*, 659.
(11) Adachi, K.; Itoh, S.; Nishi, I.; Kotaka, T. *Macromolecules* **1990**, *23*, 2554.
(12) (a) Watanabe, H.; Yamazaki, M.; Yoshida, H.; Adachi, K.; Kotaka, T. *Macromolecules* **1991**, *24*, 5365. (b) Watanabe, H.; Yamazaki, M.; Yoshida, H.; Kotaka, T. *Macromolecules* **1991**, *24*, 5372.
(13) Doi, M.; Edwards, S. F. *The Theory of Polymer Dynamics*; Clarendon: Oxford, U.K., 1986.
(14) Pearson, D. S. *Rubber Chem. Technol.* **1987**, *60*, 440.
(15) Graessley, W. W. *Adv. Polym. Sci.* **1982**, *47*, 67.
(16) Klein, J. *Macromolecules* **1978**, *11*, 852.
(17) Watanabe, H.; Tirrell, M. *Macromolecules* **1989**, *22*, 927.
(18) (a) Jarry, J. P.; Monnerie, L. *Macromolecules* **1979**, *12*, 316. (b) Tassin, J. F.; Monnerie, L.; Fetters, L. J. *Macromolecules* **1988**, *21*, 2404. (c) Lantman, C. W.; Tassin, J. F.; Monnerie, L.; Fetters, L. J.; Helfand, E.; Pearson, D. *Macromolecules* **1989**, *22*, 1184. (d) Tassin, J. F.; Baschwitz, A.; Moise, J. Y.; Monnerie, L. *Macromolecules* **1990**, *23*, 1879.
(19) (a) Kornfield, J.; Fuller, G.; Pearson, D. *Macromolecules* **1989**, *22*, 1334. (b) Ylitalo, C. M.; Fuller, G.; Abetz, V.; Stadler, R.; Pearson, D. *Rheol. Acta* **1990**, *29*, 543. (c) Ylitalo, C. M.; Kornfield, J.; Fuller, G.; Pearson, D. *Macromolecules* **1991**, *24*, 749. (d) Kornfield, J.; Fuller, G.; Pearson, D. *Macromolecules* **1992**, *25*, 5429.
(20) Yoshida, H.; Watanabe, H.; Adachi, K.; Kotaka, T. *Macromolecules* **1991**, *24*, 2981.
(21) Watanabe, H.; Urakawa, O.; Kotaka, T. *Macromolecules* **1993**, *26*, 5073.
(22) Stockmayer, W. H. *Pure Appl. Chem.* **1967**, *15*, 539.
(23) (a) Baur, M. E.; Stockmayer, W. H. *J. Chem. Phys.* **1965**, *43*, 4319. (b) Stockmayer, W. H.; Burke, J. J. *Macromolecules* **1969**, *2*, 647.
(24) Imanishi, Y.; Adachi, K.; Kotaka, T. *J. Chem. Phys.* **1988**, *89*, 7585: see references therein for earlier work on polydisperse PI chains.
(25) Yoshida, H.; Adachi, K.; Watanabe, H.; Kotaka, T. *Polym. J. (Jpn.)* **1989**, *21*, 863.
(26) Adachi, K.; Yoshida, H.; Fukui, F.; Kotaka, T. *Macromolecules* **1990**, *23*, 3138.
(27) Adachi, K.; Nishi, I.; Doi, H.; Kotaka, T. *Macromolecules* **1991**, *24*, 5843.
(28) Boese, D.; Kremer, F.; Fetters, L. J. *Macromolecules* **1990**, *23*, 829; **1990**, *23*, 1826.
(29) Patel, S. S.; Takahashi, K. M. *Macromolecules* **1992**, *25*, 4382.
(30) Cole, R. H. *J. Chem. Phys.* **1965**, *42*, 637.
(31) (a) Equation 12 is obtained on the basis of the theory of rubber elasticity that does not consider an orientational coupling[18,19] between the monomeric segments of the probe and matrix chains. However, the matrix chains are much shorter than the probe chain in most of the blends examined in this paper. For such cases, the matrix chains have already relaxed and are in an isotropic state at time scales of terminal relaxation of the probe chain. The orientational coupling with such isotropic matrices cannot effectively change the probe motion. In addition, theoretical analyses[31b-d] indicate that the orientational coupling generally has very small effects on slow viscoelastic relaxation. (The coupling is negligibly small for large, coarse-grained segments.[31d]) Thus, we can generally use eq 12 to calculate low-ω viscoelastic quantities of the probe chains. (b) Doi, M.; Pearson, D. S.; Kornfield, J.; Fuller, G. *Macromolecules* **1989**, *22*, 1448. (c) Watanabe, H.; Kotaka, T.; Tirrell, M. *Macromolecules* **1991**, *24*, 201. (d) Doi, M.; Watanabe, H. *Macromolecules* **1991**, *24*, 740.
(32) DiMarzio, E. A.; Bishop, M. *J. Chem. Phys.* **1974**, *60*, 3802.
(33) Urakawa, O.; Watanabe, H.; Kotaka, T., manuscript in preparation for publication in *Macromolecules*.
(34) (a) For examination of M_{PI} dependence of dielectric mode distribution for monodisperse bulk PI, Imanishi, Adachi, and Kotaka[24] estimated Havriliak–Negami (HN) parameters[34b] for the fast segmental (or local) relaxation, used these parameters to estimate the contribution ϵ''_{seg} of this relaxation to ϵ'' at intermediate to low ω, and subtracted ϵ''_{seg} from ϵ''. From the shape of the $\epsilon'' - \epsilon''_{seg}$ curves *obtained after this subtraction*, they concluded that the mode distribution of the global relaxation process becomes broader with increasing M_{PI}. However, the HN equation used in the subtraction does not work at low ω where the global relaxation is observed: ϵ''_{seg} described by this equation does not exhibit the characteristic terminal behavior, $\epsilon''_{seg} \propto \omega$, but depends more weakly on ω even for $\omega \to 0$, meaning that ϵ''_{seg} represented by the HN equation unreasonably has an infinitely long τ_1. Thus, the

broadening of the relaxation mode distribution concluded in ref 24 appears to be an artifact due to the use of the HN equation in an entire range of ω. In addition, at short time scales, the segmental and global relaxation modes are coupled and not necessarily separable, meaning that the subtraction itself is questionable.[12] Thus, in Figure 6 of this paper, we made no artificial subtraction for the ϵ'' curves and compared them only at low ω where the contribution of the segmental relaxation to ϵ'' is negligibly small in any way. As seen there, the mode distribution is universal and insensitive to M_{PI} at those ω. (b) Havriliak, S.; Negami, S. *J. Polym. Sci., Part C* **1966**, *14*, 99.

(35) As the matrix chains become extremely short and behave just as a low molecular weight solvent, the mode distribution for the probe PI chains becomes narrower than that seen in Figure 6.[33] This change is not related to the entanglement and/or CR effects examined in this paper and is discussed elsewhere.[33]

(36) The segmental mode contribution to ϵ'' is negligibly small at ω examined in Figure 2. Thus, $\Delta\epsilon$ for the global relaxation is evaluated from the integration of the ϵ'' data shown there.

(37) The power law dependence of τ on M_{mat} and M_{probe} (eq 33) is observed only in a narrow range of $M_{mat} \ll M_{probe}$.[3-6] With increasing M_{mat}, τ becomes more weakly dependent on M_{mat} and more strongly dependent on M_{probe}.[4-6]

(38) This τ_1/τ_{CR} ratio ($\cong 1/3.5$) was evaluated from the data on PI/PI binary blends.[11]

(39) The relaxation intensity $\Delta\epsilon$ (Figure 7) is dominated by the slow dielectric modes. Thus, the interchain correlation that might contribute to fast dielectric relaxation of bulk PI chains does not affect the $\Delta\epsilon$ values evaluated for these chains.

(40) (a) A Zimm-type CR model has the sinusoidal eigenfunctions[40b] and also fails to describe the actual F_p and f_p (Figures 9 and 10). (b) See, for example: Yamakawa, H. *Modern Theory of Polymer Solutions*; Harper & Row, New York, 1971; Chapter 6.

(41) (a) Verdier, P. H.; Stockmayer, W. H. *J. Chem. Phys.* **1962**, *36*, 227. (b) Orwoll, R. A.; Stockmayer, W. H. *Adv. Chem. Phys.* **1969**, *15*, 305.